

**A non-intrusive evaluation method for tumor-targeting characteristics of nanomedicines based on *in vivo* near-infrared fluorescence imaging - Supplementary materials**

**1. Supplementary methods**

**1.1. Materials and nanomedicines**

Dulbecco's phosphate buffered saline was purchased from Lonza (MD, USA). Hyaluronic acid (HA, molecular weight 100k Da on average) was purchased from Aladdin Industrial Inc. (Shanghai, China). Dimethyl sulfoxide, (-)-gossypol (AT101), trypsin-EDTA solution, and Dulbecco's modified Eagle's medium (DMEM) were purchased from Sigma-Aldrich (MO, USA). Fetal bovine serum, penicillin, streptomycin, and 1,1'-dioctadecyl-3,3',3',3'- tetramethylindotricarbocyanine-iodide (DiR) were purchased from Invitrogen (NY, USA). All reagents were used without further purification. Stearic acid-grafted polyethyleneimine (PgS, molecular weight about 12k Da on average), PEG<sub>5k</sub>-embelin<sub>2</sub> conjugate (PEG-EB<sub>2</sub>), PEG<sub>5k</sub>-vitamine E<sub>2</sub> conjugate (PEG-VE<sub>2</sub>), and cationized stearic acid-grafted starch (CSaSt, molecular weight about 20k Da on average) were prepared according to our previous reports<sup>1-5</sup>. The chemical structures of PgS, PEG-EB<sub>2</sub>, PEG-VE<sub>2</sub>, and CSaSt are shown in the supplementary Fig. S1. PgSHA nanoparticles, PEG-EB<sub>2</sub> and PEG-VE<sub>2</sub> micelles, and CSaStHA nanoparticles were prepared via a modification of our previously reported methods<sup>4,5</sup>.

**1.2. Cell culture**

PC-3 and CL-1 prostate cancer cell lines, HCT 116 colon cancer cell line, and MDA-MB-231 breast cancer cell line were provided by the Department of Molecular Biosciences, University of Kansas, and have passed the tests for mycoplasma contamination. The cells were grown in complete DMEM supplemented with 10% (w/w) FBS and penicillin/streptomycin (76 and 36 U mL<sup>-1</sup>, respectively), and

were incubated under 5% CO<sub>2</sub> at 37 °C in a cell incubator (MCO-18AIC, Sanyo, Japan).

### 1.3. Animal tumor models

All animal experiments were performed in compliance with the guidelines for use and care of animals in University of Kansas and were approved by the Institutional Animal Care and Use Committee. Immunodeficient animals are suitable for tumor cell growth. NOD.CB17-*Prkdc*<sup>scid</sup> (SCID) mice and NCI athymic NCr-nude mice from Harlan Laboratories (Denver, CO) were used to established tumor models and were kept under standard housing conditions. After alcohol preparation of the skin, two-month-old to three-month-old mice were *s.q.* injected with suspension of one kind of cells in DMEM using a sterile 23-gauge needle. Approximately 200 μL DMEM containing 1×10<sup>6</sup> cells for each injection was used. Tumors in the mice grew to predetermined sizes before the mice were ready for the *in vivo* imaging or drug efficacy experiments.

### 1.4. Preparation and characterization of nanomedicines

The preparation scheme of DiR/(-)-gossypol-loaded PgSHA nanoparticles (DiR-PgSHA and (-)-G-PgSHA) is shown in Fig. S2A. The preparation of PgSHA nanoparticles was a modification of our previously reported methods<sup>4,5</sup>. Briefly, 0.1 mg DiR or 10 mg (-)-gossypol were codissolved with 5.2 mg PgS in 2 mL ethanol. The mixture solution was added to 5 mL deionized water under vigorous stirring to form drug/dye-loaded micelles. The solution was then filtered using a glass funnel and dialyzed against deionized water using a dialysis membrane (MWCO 3.5 kDa) to remove the free DiR/(-)-gossypol and organic solvent. Afterwards, the micelle solution was dripped to 15 mL of 0.5% HA solution under vigorous stirring to form DiR-PgSHA or (-)-G-PgSHA. The DiR-PgSHA or (-)-G-PgSHA solutions were concentrated to a determined volume by vaporization before further use. Blank PgSHA nanoparticles were prepared similarly without the drug or dye.

DiR-loaded PEG-EB<sub>2</sub> and PEG-VE<sub>2</sub> micelles were similarly prepared according to our previous reports<sup>1,6</sup>. The preparation scheme of drug/NIR fluorescent dye-loaded PEG-EB<sub>2</sub> and PEG-VE<sub>2</sub> micelles is shown in Fig. S3A. Briefly, DiR was added to PEG-EB<sub>2</sub> or PEG-VE<sub>2</sub> in chloroform with a dye/carrier molar ratio of 1/100. The chloroform was removed under vacuum overnight to form a thin and dry film of dye/carrier mixture. DiR-loaded micelles were then formed by suspending the film in DPBS. DiR concentration was 50 nmol mL<sup>-1</sup> for both the DiR-loaded PEG-EB<sub>2</sub> and PEG-VE<sub>2</sub> micelles.

The preparation of DiR-loaded CSaStHA nanoparticles was the modification of our reported method<sup>3</sup>. DiR (10 mmol L<sup>-1</sup> in ethanol) was added to CSaSt (0.2 mmol saccharide units mL<sup>-1</sup> in DMSO) with a dye/saccharide ratio of 1/10. The mixture was added to deionized water, and was then dialyzed (using a 3500 Da MWCO dialysis membrane) against water in the dark to get rid of the organic solvents. The DiR-loaded CSaSt micelle in water was concentrated to a determined volume by vaporization in the dark, and was then added to DPBS containing 0.5% (w/w) HA. The final concentration of DiR in the solution was 50 nmol mL<sup>-1</sup>.

The morphology of DiR-loaded nanocarriers was studied using transmission electron microscopy (TEM) after negative staining. The dynamic size distribution and zeta-potential of different nanocarriers were measured using a Malvern instrument (Nano-ZS90, Malvern, UK).

### **1.5. NIR fluorescence imaging of nanomedicines *in vivo* and *ex vivo***

The *in vivo* tumor-targeted characteristics of DiR nanomedicines were studied and compared with free DiR. This was *i.v.* injected to SCID mice bearing CL-1, HCT-116, and MDA-MB-231 tumors. Each mouse was given 200  $\mu$ L of DiR-loaded nanoparticles containing 10 nmol DiR. For *in vivo* imaging of free DiR, one mouse was *i.v.* injected with 200  $\mu$ L ethanol/PBS (1:4, v/v) solvent mixture containing 10 nmol DiR. The hairs on the ventral side of mice were removed before imaging. At different time points, the

biodistribution of DiR-loaded nanocarriers in the mouse was measured using a Carestream molecular imaging system (In-Vivo MS FX PRO, Carestream Health, Inc.), with excitation and emission at 750 and 830 nm, respectively. Mice were euthanized after 72 or 96 h when the DiR signal started to diminish. Organs and tumors of the mice were then obtained for *ex vivo* imaging. All imaging processes used the same imaging settings, which were 200 mm × 200 mm field of view (FOV), 2.8 f-stop, and 60 s exposure time. The settings were determined based on the injected dose of the dye and the number of mice for imaging. The f-stop of 2.8 and exposure time of 60 s ensured that the fluorescence from DiR in the tumors was well observed during the imaging process.

#### **1.6. Data processing of *in vivo* and *ex vivo* NIR fluorescence imaging for quantitative evaluation**

The unit of fluorescence intensity of all the obtained images was converted to “photons/second per square mm” using the ‘Image Math’ function of Carestream molecular imaging software (Carestream Health, Inc) based on a 200 mm × 200 mm FOV. The *in vivo* absolute fluorescence intensity of the whole body, tumor regions, and *ex vivo* absolute fluorescence intensity of tumors and organs in the images were quantified by the Carestream molecular imaging software using the function of ‘Manual Regions of Interest’.

#### **1.7. Calculation of the fluorescence percentage of injected dose per gram (%ID/g) of each tissue**

The *in vitro* imaging of DPBS containing different amounts of DiR-loaded nanocarriers was performed and used to create calibration curves for each DiR-loaded nanocarrier. Examples of the resultant image and the calibration curves were shown in Fig. S7. Nevertheless, it is also important to measure the non-specific signals of free dye as a control of the dye-loaded nanocarriers. As DiR is hydrophobic, it was dissolved well in different organic solvents and gave strong emission of fluorescence after proper excitation (Fig. S8A). In aqueous environment however, DiR gave a weak fluorescence signal due to poor

solubility and quenching effect. The 20% ethanol was used to help DiR dissolve into DPBS. The calibration curves for free DiR were summarized in Fig. S8B. Free DiR showed good linearity for the organic solvents and poor linearity for the 20% ethanol in DPBS, which correlates with the result that free DiR in PC-3 tumor-bearing mouse had very low signal intensity (Fig. 2). This demonstrated the important role of nanocarriers in protecting their payloads from external environment, prolonging their retention in the body, and facilitating their accumulation in specific regions of the body.

To calculate the fluorescence percentage of injected dose per gram (%ID/g) of each tissue, calibration curves were made for each DiR-loaded nanocarrier in the first place. 50  $\mu$ L DPBS containing different amount of DiR-loaded nanocarriers was added in each well of a 96-well plate before *in vitro* imaging, using the same settings with that of *in vivo* imaging. The calibration curves were then produced by the software Prism 5 (GraphPad Software Inc., California, USA) using the fluorescence intensity of each well obtained by the imaging software. The formulae attached in the calibration curves were produced using the software Microsoft Excel (Microsoft Inc., Washington State, USA). The calibration curves of free DiR in different solvents were obtained in the same way. In the *ex vivo* images, ROI was set as part of each tissue to ensure that the fluorescent intensity of selected part was within the linear range of calibration curve. The %ID/g of each selected part of tissue was then calculated as follows:

$$\%ID/g = \frac{M_{DiR}}{ID \times W_{Tissue}} \times 100\% \quad (1)$$

where  $M_{DiR}$  is the amount (nmol) of DiR residue in selected tissue, ID is the injected amount (nmol) of DiR, and  $W_{Tissue}$  is the weight (g) of each tissue.

### 1.8. *In vivo* tumor inhibition of (-)-G-PgSHA

PC-3 tumor model was used to study the tumor growth inhibition of (-)-G-PgSHA. When the tumors

on the mice grew to an average size of about 50 mm<sup>3</sup>, the mice were randomly divided into 3 groups (n = 8) and were *i.v.* injected with 1) PBS (blank control), 2) (-)-G-PgSHAs (10 mg (-)-gossypol/kg), and 3) 10 mg/kg free (-)-gossypol. Each mouse was treated twice a week, for three weeks. All animals were sacrificed 1 month after the first administration. The tumor tissues were removed and sectioned, and then stained by hematoxylin and eosin and histologically observed.

The tumor growth inhibition rate (IR) was calculated as follows:

$$\text{IR}(\%) = \left(1 - \frac{T}{C}\right) \times 100\% \quad (2)$$

where  $T$  is the average tumor volume (mm<sup>3</sup>) of test group when the control group tumors reach 800 mm<sup>3</sup> (on average), and  $C$  is the average tumor volume (mm<sup>3</sup>) of the control group measured at the same time.

## 1.9. Statistical analysis

The data of *in vivo* imaging and tumor growth were analyzed using two-way ANOVA. The data of *ex vivo* imaging were analyzed using Student's t-test. The data were analyzed and presented using Prism 5.0 software (GraphPad Prism, CA, USA). Difference with  $P$  value below 0.05 was considered statistically significant.

## 2. Supplementary results and discussion

### 2.1. Preparation and characterization of nanomedicines

The TEM photo in Fig. S2B shows that, DiR-PgSHA nanoparticles had homogeneous and spherical shape. The nanoparticles had an average particle size of around 130 nm, with a negative charge of around -30 mV (Fig. S2B), due to the shield of negative-charged hyaluronic acid. PEG-EB<sub>2</sub> micelles, PEG-VE<sub>2</sub> micelles, and CSaStHA nanoparticles were all sub-100 nm on average (Fig. S3B). Both PEG-EB<sub>2</sub> and PEG-VE<sub>2</sub> micelles had small charges around zero, while CSaStHA nanoparticles had a negative zeta-

potential, which was also due to the hyaluronic acid on the surface. The results of each nanoparticle were close to those of its according blank and drug-loaded nanoparticles as previously reported <sup>1,3-6</sup>, which indicated that the encapsulation of DiR did not significantly affect the appearance of these nanoparticles.

## References

1. J. Lu, Y. Huang, W. Zhao, R. T. Marquez, X. Meng, J. Li, X. Gao, R. Venkataramanan, Z. Wang and S. Li, *Biomaterials*, 2013, **34**, 1591-1600.
2. J. Lu, Y. Huang, W. Zhao, Y. Chen, J. Li, X. Gao, R. Venkataramanan and S. Li, *Mol. Pharm.*, 2013, **10**, 2880-2890.
3. K. Li, H. Liu, W. Gao, M. Chen, Y. Zeng, J. Liu, L. Xu and D. Wu, *Biomaterials*, 2015, **39**, 131-144.
4. H. Liu, K. Li, L. Xu and D. Wu, *J. Nanopart. Res.*, 2014, **16**.
5. H. Liu, K. Li, L. Lan, J. Ma, Y. Zeng, L. Xu and D. Wu, *J. Mater. Chem. B*, 2014, **2**, 5238-5248.
6. Y. Huang, J. Lu, X. Gao, J. Li, W. Zhao, M. Sun, D. B. Stolz, R. Venkataramanan, L. C. Rohan and S. Li, *Bioconj. chem.*, 2012, **23**, 1443-1451.

### 3. Supplementary Figures and Figure Captions

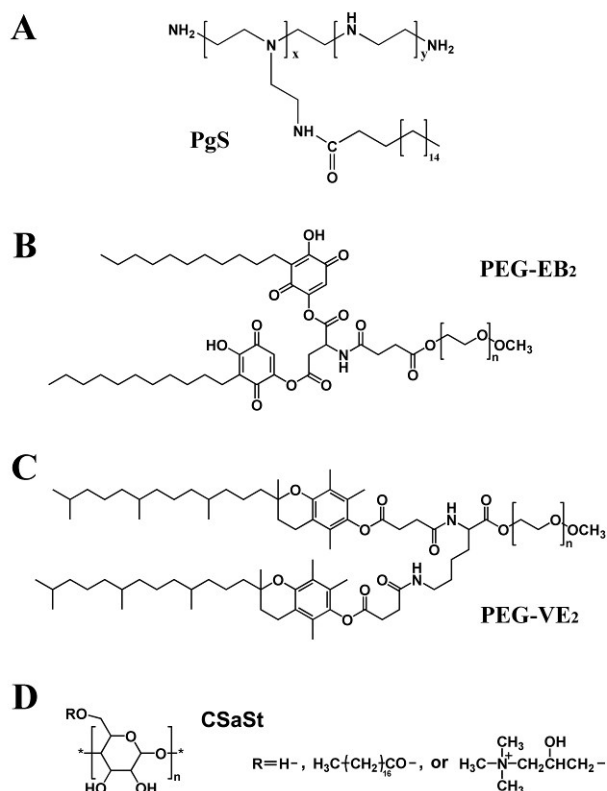


**Figure S1.** Chemical structures of A) stearic acid-grafted polyethyleneimine (PgS); B) PEG<sub>5k</sub>-embelin<sub>2</sub> conjugate (PEG-EB<sub>2</sub>); C) PEG<sub>5k</sub>-vitamine E<sub>2</sub> conjugate (PEG-VE<sub>2</sub>); and D) cationized stearic acid-grafted starch (CSaSt).

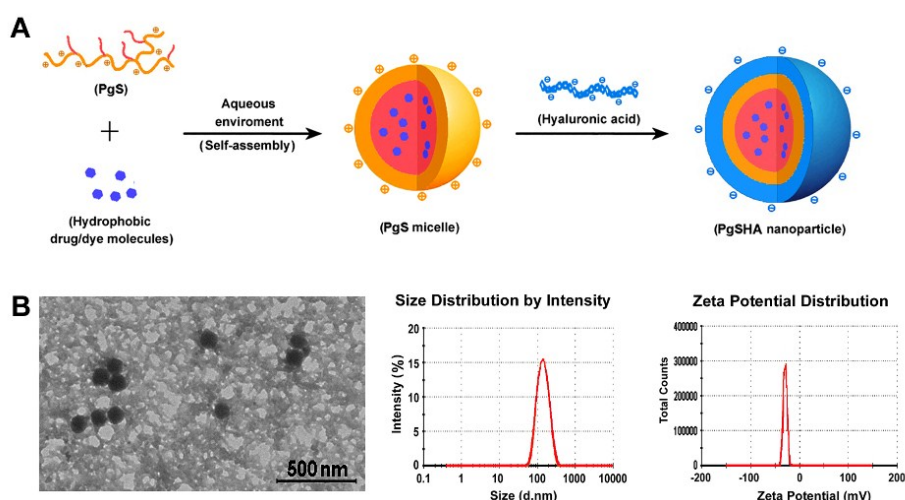


**Figure S2.** A) Scheme of preparation of drug/NIR fluorescent dye-loaded PgSHA nanoparticle. B) The TEM images, dynamic size distribution and zeta-potential of PgSHA nanoparticles. The PgSHA nanoparticles are in spherical shape with an average size of about 130 nm and zeta-potential of about -29 mV.

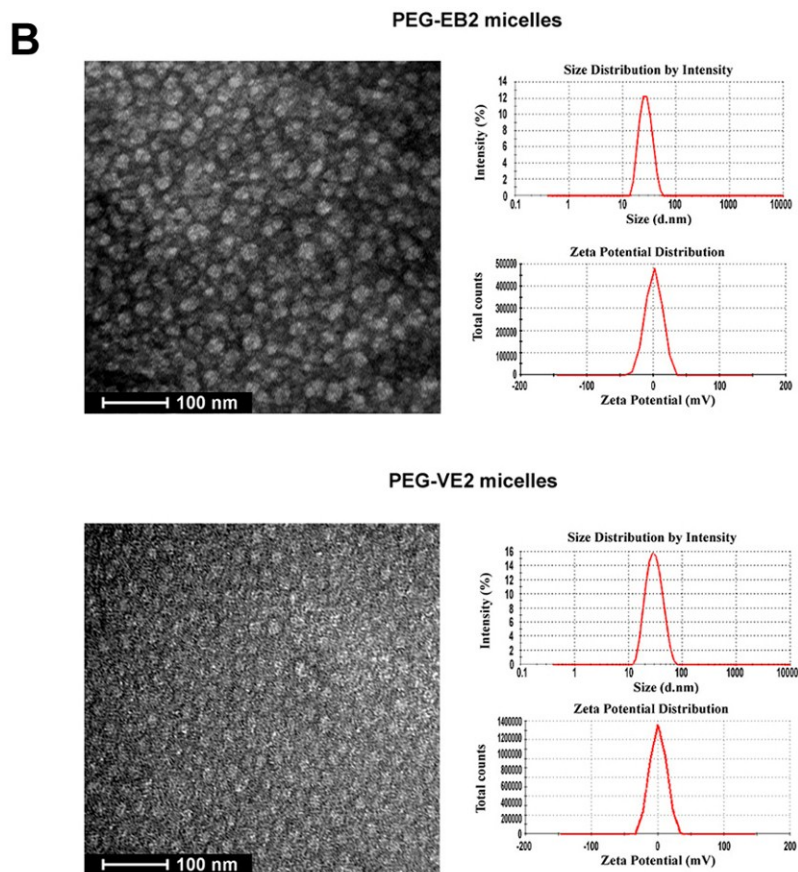
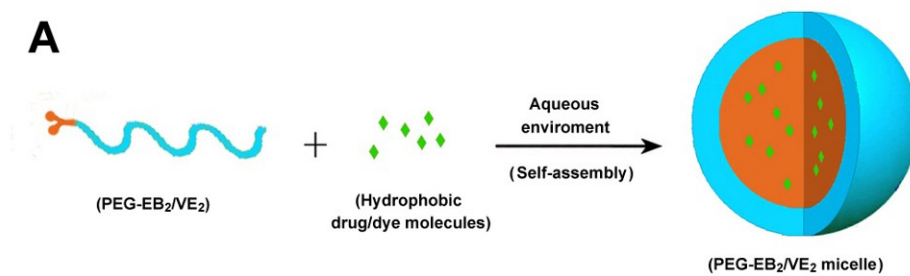


**Figure S3.** A) Scheme of preparation of drug/NIR fluorescent dye-loaded PEG-EB<sub>2</sub> and PEG-VE<sub>2</sub> micelles. B) The TEM images, dynamic size distribution and zeta-potential of different micelles. Both micelles have an average size of sub-100 nm.

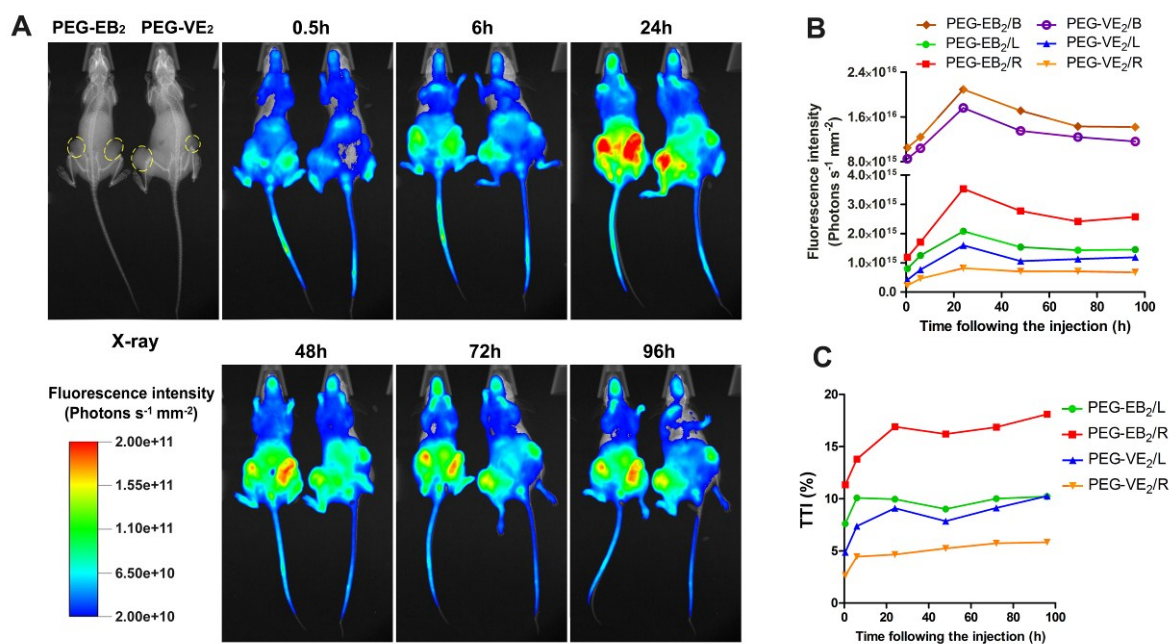


**Figure S4.** *In vivo* imaging of HCT 116 tumor-bearing female SCID mice injected with DiR-encapsulated micelles. A) *In vivo* NIR fluorescence imaging of mice injected with DiR-encapsulated PEG-EB<sub>2</sub> (left) and PEG-VE<sub>2</sub> (right) micelles at different time post-injection. Tumor regions were indicated by dashed yellow circles. B) DiR fluorescence intensity of tumor regions and whole bodies. “L”, “R”, and “B” in the legend refer to left tumor, right tumor, and whole body, respectively. C) The tumor-targeting index (TTI) of the micelles in each tumor region at different time points. “L” and “R” in the legend refer to left tumor and right tumor, respectively.

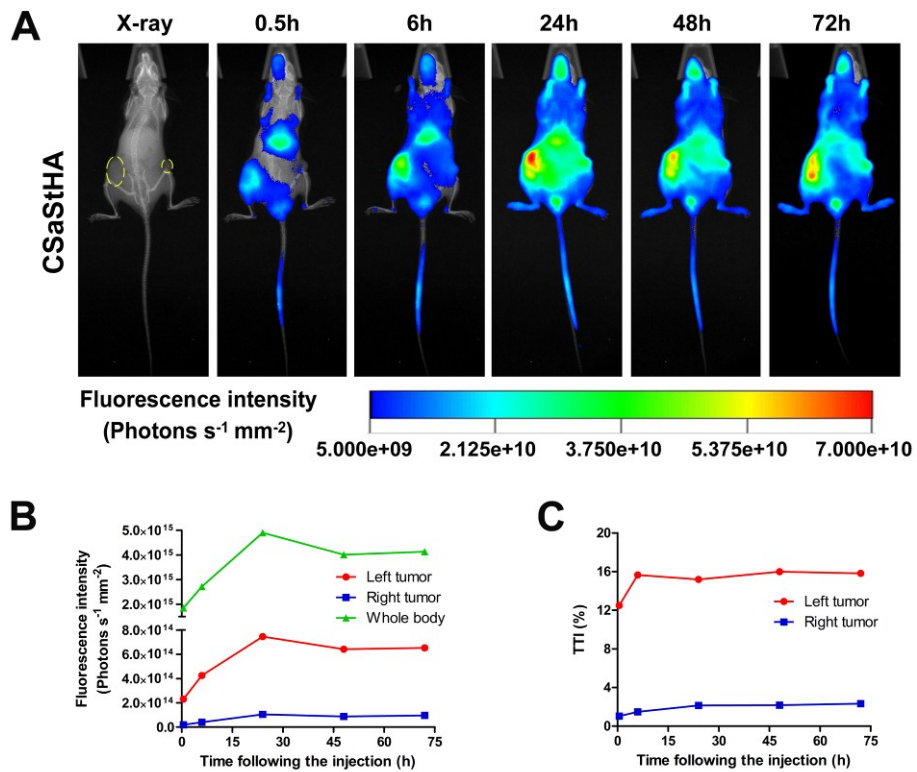


**Figure S5.** A) *In vivo* imaging of female SCID mouse that bore two MDA-MB-231 tumors with different sizes. The mouse was injected with DiR-encapsulated CSaStHA nanoparticles. Tumors were indicated by dashed yellow circles. The DiR signal intensity in the bigger tumor was strong. In the small tumor, however, DiR signal was very weak, due to the immature vasculature in small tumor that made it difficult for sub-100 nm nanocarriers to enter the tumor. B) The DiR intensity and C) the TTI of the nanoparticle in each tumor region quantified the great DiR intensity difference between the two tumors.

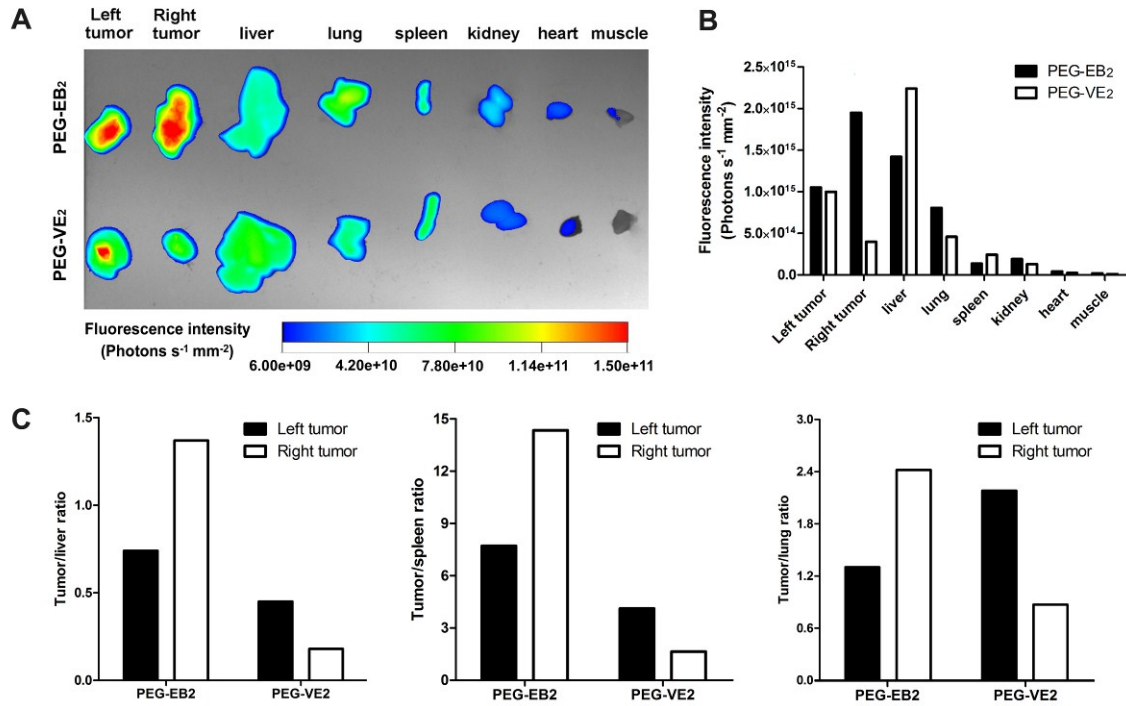


**Figure S6.** *Ex vivo* imaging of HCT 116 tumor-bearing female SCID mice injected with DiR-encapsulated micelles. A) *Ex vivo* imaging of tumors and organs from each mouse. B) The absolute DiR signal intensity of tumors and organs from each mouse. C) Ratios of DiR signal intensity of tumors to liver (left), spleen (middle) and lung (right).

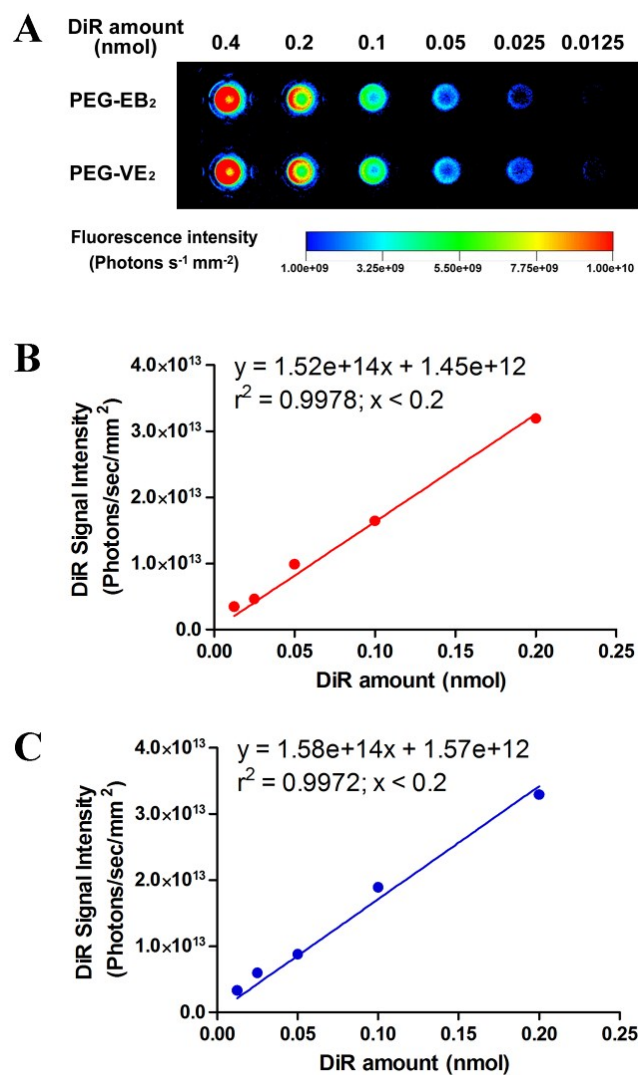


**Figure S7.** A) *In vitro* NIR fluorescence imaging of DiR in different micelles for calibration curves. B) Standard curves of DiR loaded in PEG-EB<sub>2</sub> micelles. C) Standard curves of DiR loaded in PEG-VE<sub>2</sub> micelles.

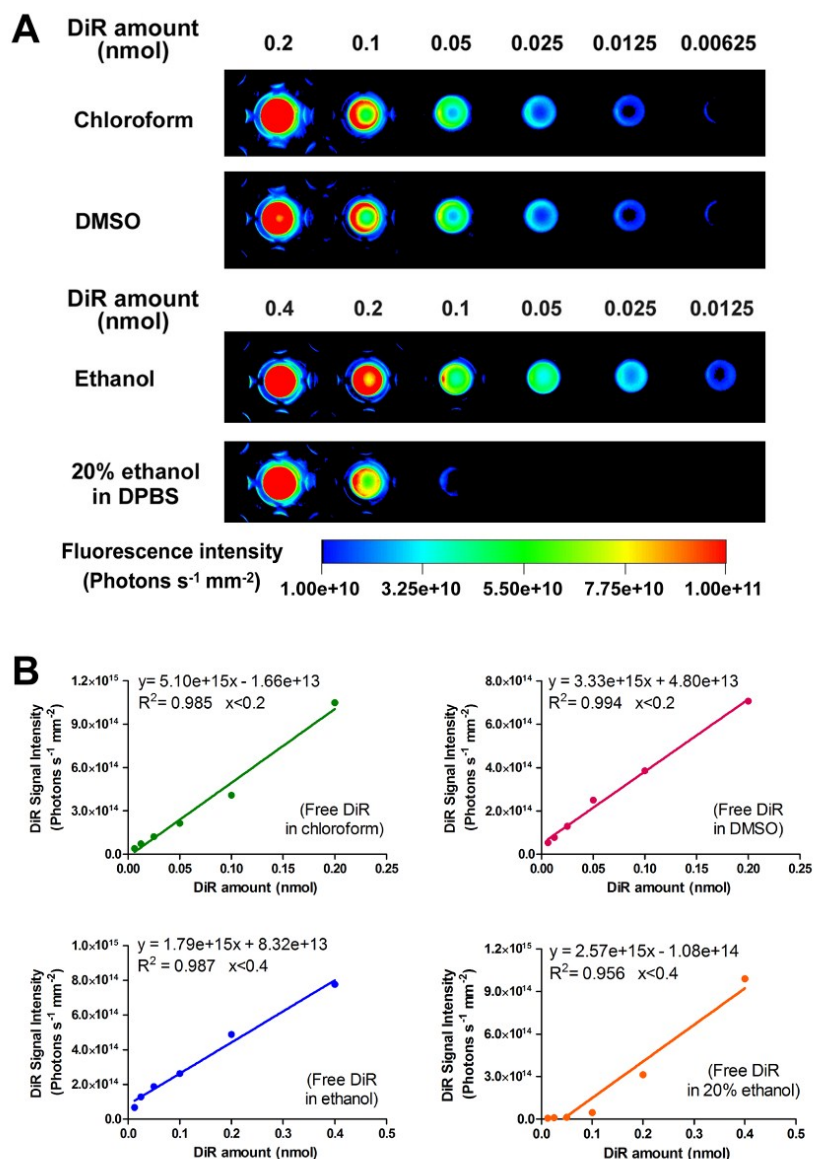


**Figure S8.** A) *In vitro* imaging of free DiR in different solvents. B) Standard curves of free DiR in chloroform (upper left), DMSO (upper right), ethanol (lower left), and 20% ethanol (lower right). The poor DiR signal intensity in 20% ethanol was due to the quenching effect of aqueous solvent on hydrophobic DiR molecules.

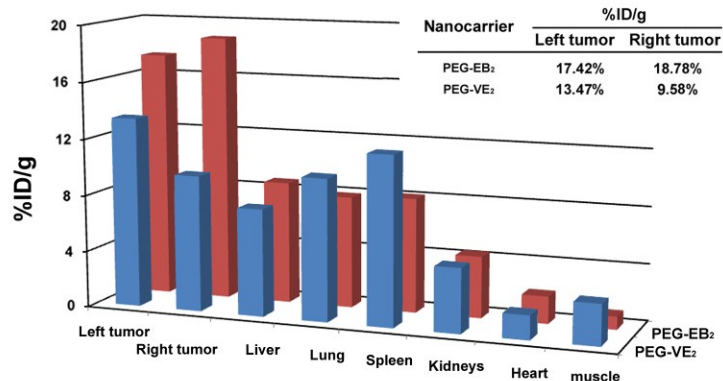


**Figure S9.** Biodistribution of DiR in tissues as indicated by %ID/g tissue. The exact values for tumors were presented on the upper right.

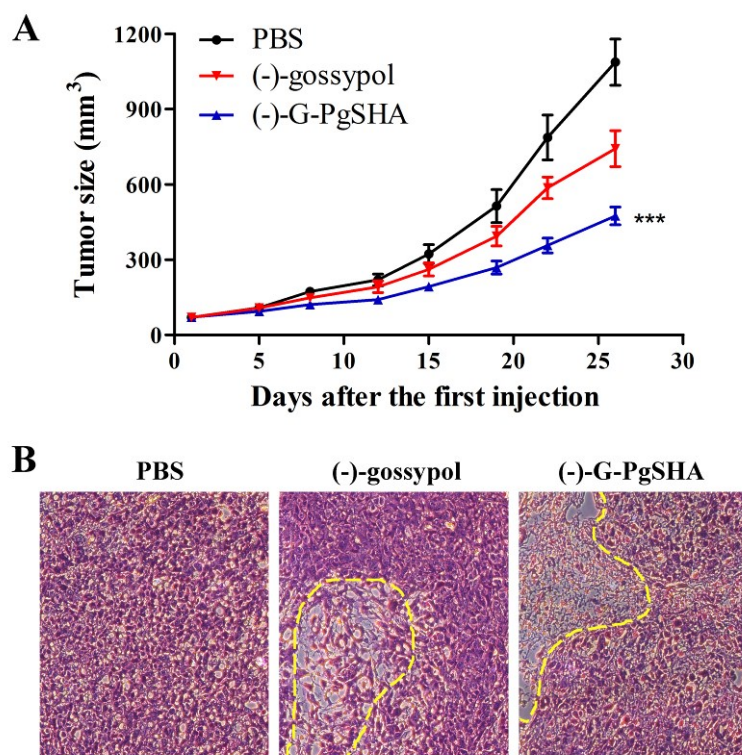


**Figure S10.** A) *In vivo* tumor growth curves of nude mice inoculated *s.q.* with PC-3 cells on the back. Mice were treated with PBS, free (-)-gossypol (10 mg/kg), and (-)-G-PgSHA (10 mg drug/kg), respectively. Data are shown as mean  $\pm$  SEM ( $n = 8$ ). \*\*\* $P < 0.001$  as compared with both PBS group and (-)-gossypol group after day 22. B) Pathological section images of tumor tissue from PC-3 tumor-bearing nude mice with different treatment. Samples were stained using hematoxylin and eosin. Magnification was 200 $\times$ .